

A Fuzzy Neural Network Approach to Adaptive Robust Nonsingular Sliding Mode Control for Predefined-Time Tracking of A Quadrotor

Yongjun He, Lin Xiao, Zidong Wang, *Fellow, IEEE*, Qiuyue Zuo, and Linju Li

Abstract—In this paper, a novel adaptive robust predefined-time nonsingular sliding mode control (ARPTNSMC) scheme is investigated, which aims to achieve fast and accurate tracking control of a quadrotor subjected to external disturbance. Inspiration is drawn from a fuzzy neural network that is constructed by fuzzy logic and zeroing neural network (ZNN). Distinct from most sliding mode control (SMC) approaches, a nonsingular sliding mode surface is formulated by employing a general ZNN and a differentiable predefined-time activation function. Furthermore, for the compensation of external disturbance, a dynamic adaptive parameter and a fuzzy adaptive parameter are designed in the control law. The fuzzy adaptive parameter, generated by the Takagi-Sugeno fuzzy logic system, is incorporated to enhance the robustness while reducing the chattering phenomena resulting from the discontinuous sign function. Theoretical proofs are provided to demonstrate the predefined-time convergence and robustness of the closed-loop system. Lastly, two trajectory tracking examples are offered to validate the convergence, robustness, and low-chattering characteristics of the closed-loop system under the developed ARPTNSMC scheme.

Index Terms—Fuzzy neural network, predefined-time convergence, Takagi-Sugeno fuzzy logic system, zeroing neural network, nonsingular sliding mode control, quadrotor.

I. INTRODUCTION

Quadrotor unmanned aerial vehicles (UAVs) are extensively utilized in various fields of science and engineering because of their straightforward design, minimal maintenance costs, and outstanding hovering precision [1]. Quadrotors are employed in a range of applications including surveying, mapping, searching, and rescuing [2], [3]. In response to the control complexities of quadrotors, diverse control strategies have been developed, which include backstepping control [4], model predictive control [5], and sliding mode control (SMC) [6]. Notably, SMC is recognized as an effective strategy for quadrotors, particularly due to its robustness against parameter variations and disturbances [6]–[8].

In recent decades, considerable research has focused on the convergence and robustness of quadrotor systems. For example, an adaptive sliding mode control has been developed

in [9] for the finite-time stabilization of UAV systems. The tracking problem of a quadrotor UAV under wind disturbances has been dealt with in [10] by using an adaptive super-twisting terminal SMC strategy, confirming the finite-time reachability of sliding surfaces. However, the fixed-time convergent schemes are significantly affected by initial conditions. In response, a fixed-time SMC scheme has been proposed in [11] for a quadrotor UAV under external disturbances, ensuring the fixed-time convergence of states. Nevertheless, the coupling relationships (between parameters that determine the upper bound of convergence time in these finite-time or fixed-time SMC strategies) can adversely affect the adjustment of practical convergence performance. Although a particle swarm algorithm for parameter optimization in an SMC has been put forward in [12], its performance is contingent on the choice of group size and can substantially increase computational costs [13]. Therefore, the development of a robust predefined-time SMC scheme, with its convergence time controllable by an independent parameter, is crucial.

Neural networks, particularly the zeroing neural network (ZNN), a variant of the recurrent neural network, are extensively used in engineering due to their efficient parallel processing capabilities [14]–[16]. ZNN excels in dynamic problems like sensor localization [17], manipulator control [18]–[21], and chaos control [22]. Various robust ZNN models have been developed with focus on fixed-time or predefined-time convergence by using activation functions and integral designs [22]–[24]. For instance, a fixed-time robust ZNN controller for chaos synchronization and a noise-tolerant ZNN for robotic manipulator motion control have been proposed to demonstrate ZNN’s versatility and effectiveness [22], [24].

In the ZNN and SMC schemes previously discussed, system parameters are typically static. However, recent research has shown that variable parameters, such as dynamic adaptive and fuzzy adaptive parameters, can significantly enhance the convergence and robustness of systems [25]–[30]. For example, an adaptive ZNN with dynamic parameters has been developed in [25] for UAV regulation under unknown disturbances, a fuzzy-neural controller has been designed in [27] for collaborative control of multi-manipulator systems, and an adaptive ZNN utilizing the Takagi-Sugeno fuzzy logic system has been established in [28] for quadratic programming in order to achieve adaptive fixed-time convergence. Despite these advancements, the issue of chattering caused by the discontinuous sign function has been somewhat overlooked in earlier robustness research. To address this, the current

This work was supported in part by the National Natural Science Foundation of China under Grant 61866013.

Y. He, L. Xiao, Q. Zuo, and L. Li are with Hunan Provincial Key Laboratory of Intelligent Computing and Language Information Processing, Hunan Normal University, Changsha 410081, China, and also with MOE-LCSM, Hunan Normal University, Changsha 410081, China (e-mail: xiaolin860728@163.com).

Z. Wang is with Department of Computer Science, Brunel University London, Uxbridge, Middlesex, UB8 3PH, United Kingdom (e-mail: Zidong.Wang@brunel.ac.uk).

paper introduces a fuzzy adaptive parameter in conjunction with the dynamic adaptive parameter to mitigate chattering while compensating for disturbances.

Motivated by the concepts of fuzzy logic and ZNN, this paper introduces an innovative adaptive robust predefined-time nonsingular sliding mode control (ARPTNSMC) scheme through establishing a fuzzy neural network. The primary goal of this scheme is to facilitate precise position and attitude tracking of a quadrotor even in the presence of bounded disturbances. The approach involves several key steps: 1) formulation of a nonsingular sliding mode surface using a general ZNN combined with a differentiable predefined-time activation function (AF); 2) construction of a unified ZNN that incorporates both a dynamic adaptive parameter and a fuzzy adaptive parameter, effectively creating a fuzzy neural network to be employed to develop an approaching law; and 3) integration of the nonsingular sliding mode surface with the approaching law, culminating in the development of a nonsingular robust predefined-time controller. Finally, the paper presents theoretical analyses and [two illustrative examples](#) to demonstrate the effectiveness and superiority of the ARPTNSMC scheme.

This paper makes several key contributions outlined as follows.

- 1) Two novel predefined-time AFs are introduced, which ensure both the predefined-time convergence of the closed-loop system and the non-singularity of the controller.
- 2) The ARPTNSMC scheme incorporates two types of adaptive parameters, and such a dual-parameter approach significantly compensates for external disturbances. Notably, the fuzzy adaptive parameter not only enhances the system's robustness but also effectively suppresses chattering (a common issue caused by the discontinuous sign function).
- 3) The convergence and robustness of the closed-loop system under the ARPTNSMC scheme are rigorously proven, and the analyses demonstrate that the calculated convergence time is exclusively related to an independent predetermined parameter denoted as \mathcal{T}_p .
- 4) The efficacy of the ARPTNSMC scheme is further validated through butterfly-shaped trajectory [and Lissajous trajectory](#), which clearly demonstrates the scheme's predefined-time convergence and strong robustness. Furthermore, [an ablation experiment](#) is conducted to highlight the ARPTNSMC scheme's capability in chattering suppression.

The structure of the paper is organized into five distinct sections following the introduction. Section II provides the necessary preliminaries and formulates the problem. Building upon two existing ZNN schemes, Section III introduces the SMC scheme, which features the novel introduction of a dynamic adaptive parameter and a fuzzy adaptive parameter, along with two predefined-time activation functions. Section IV focuses on the theoretical analysis of the predefined-time convergence and robustness of the closed-loop system under the ARPTNSMC scheme. In Section V, [two illustrative](#)

TABLE I
LIST OF ABBREVIATIONS.

| Abbreviation | Description |
|--------------|------------------------------------------------------------------|
| AF | Activation function |
| ARPTNSMC | Adaptive robust predefined-time nonsingular sliding mode control |
| CNTSMC | Continuous nonsingular terminal sliding mode control |
| FTRZNN | Fixed-time robust zeroing neural network |
| PTAF | Predefined-time activation function |
| SMC | Sliding mode control |
| SMS | Sliding mode surface |
| TSFLS | Takagi-Sugeno fuzzy logic system |
| UAV | Unmanned aerial vehicle |
| UZNN | Unified zeroing neural network |
| ZNN | Zeroing neural network |

[examples](#) are presented to validate the theorems proposed in Section IV and demonstrate the superiority of the novel SMC scheme in terms of convergence time and anti-interference capabilities, compared to other schemes [31]–[34]. Section VI concludes the work by summarizing the key findings and contributions and suggesting possible directions for future research.

Moreover, a list of abbreviations appeared in this work is provided in Table I.

II. PRELIMINARY AND PROBLEM FORMULATION

In this section, essential definitions and lemmas are initially presented to establish the theoretical foundation. Subsequently, the focus shifts to exploring the nonlinear dynamics of an X-type quadrotor, along with its position and attitude tracking challenges.

A. Preliminary

Consider a nonlinear system

$$\dot{\boldsymbol{\xi}}(t) = -\mathbf{f}(\boldsymbol{\xi}(t)), \quad \boldsymbol{\xi}(0) = \boldsymbol{\xi}_0 \quad (1)$$

where $\boldsymbol{\xi}(t) \in \mathbb{R}^n$ represents the state and $\mathbf{f}(\cdot) : \mathbb{R}^n \rightarrow \mathbb{R}^n$ denotes a nonlinear vector function with its element being $f(\cdot) : \mathbb{R} \rightarrow \mathbb{R}$. Let the origin be an equilibrium point. Then, some definitions and lemmas are given as follows.

Definition 1 ([35]). *If there exists a real number $T_s \geq 0$ determined by $\boldsymbol{\xi}_0$ such that $\|\boldsymbol{\xi}(t)\|_2 = 0$ for all $t \geq T_s$, then*

$$T(\boldsymbol{\xi}_0) = \inf\{T_s \geq 0 : \|\boldsymbol{\xi}(t)\|_2 = 0, \forall t \geq T_s\} \quad (2)$$

is said to be the [settling time](#) of the system (1).

Definition 2 ([35], [36]). *The origin of the system (1) is finite-time stable if there exists a [settling time](#) $T(\boldsymbol{\xi}_0) < +\infty$ such that $\|\boldsymbol{\xi}(t)\|_2 = 0$ for all $t \geq T(\boldsymbol{\xi}_0)$ and any $\boldsymbol{\xi}_0 \in \mathbb{R}^n$.*

Definition 3 ([36], [37]). *The origin of the system (1) is fixed-time stable if it is finite-time stable and $T(\boldsymbol{\xi}_0) \leq \mathcal{T}_f < +\infty$ holds, where \mathcal{T}_f is unrelated to the initial state $\boldsymbol{\xi}_0$.*

Definition 4 ([36], [38]). *The origin of the system (1) is predefined-time stable if it is fixed-time stable and the time $T(\xi_0) \leq \mathcal{T}_s < +\infty$, where \mathcal{T}_s is irrelevant to the initial state and other system parameters.*

Definition 5 ([36], [37]). *The integral*

$$B(a, b) = \int_0^1 y^{a-1}(1-y)^{b-1} dy$$

is called beta function, where $a > 0$ and $b > 0$.

Lemma 1 ([39]). *For the beta function, one has*

$$B(\xi, 1 - \xi) = \frac{\pi}{\sin(\xi\pi)} = \pi \csc(\xi\pi).$$

B. Problem Formulation

According to the Newton-Euler equations [40], [41], the dynamics of the X-type quadrotor are modeled as

$$\begin{cases} \ddot{x} = \frac{1}{m} (-K_{dx}\dot{x} + (s_\phi s_\psi + c_\phi s_\theta c_\psi) u_3), \\ \ddot{y} = \frac{1}{m} (-K_{dy}\dot{y} + (-s_\phi c_\psi + c_\phi s_\theta s_\psi) u_3), \\ \ddot{z} = \frac{1}{m} (-K_{dz}\dot{z} + c_\phi c_\theta u_3) - g, \\ \ddot{\phi} = \frac{1}{J_x} \left((J_y - J_z) \dot{\theta} \dot{\psi} - J_r \bar{\Omega} \dot{\theta} - K_{fx} \dot{\phi} + u_4 \right), \\ \ddot{\theta} = \frac{1}{J_y} \left((J_z - J_x) \dot{\phi} \dot{\psi} + J_r \bar{\Omega} \dot{\phi} - K_{fy} \dot{\theta} + u_5 \right), \\ \ddot{\psi} = \frac{1}{J_z} \left((J_x - J_y) \dot{\phi} \dot{\theta} - K_{fz} \dot{\psi} + u_6 \right), \end{cases} \quad (3)$$

where m is the mass of the quadrotor; $[x, y, z]^T$ is the position of the quadrotor's center of mass; ϕ , θ , and ψ represent the roll, pitch, and yaw angles, respectively; $s_{(\cdot)}$ and $c_{(\cdot)}$ signify sine function and cosine function; K_{dx} , K_{dy} , and K_{dz} are the translation air drag coefficients, respectively; g represents the gravity acceleration; J_x , J_y , and J_z denote the moment of inertia in the X-, Y-, and Z-directions; J_r is the rotational inertia of each rotor; $\bar{\Omega} = \sum_{i=1}^4 (-1)^{i+1} w_i$ with w_i representing the angular speed of the i -th rotor; K_{fx} , K_{fy} , and K_{fz} represent aerodynamic friction coefficients; and the control input is denoted by

$$\begin{bmatrix} u_3 \\ u_4 \\ u_5 \\ u_6 \end{bmatrix} = \begin{bmatrix} K_l & K_l & K_l & K_l \\ \frac{\sqrt{2}}{2} l K_l & \frac{\sqrt{2}}{2} l K_l & -\frac{\sqrt{2}}{2} l K_l & -\frac{\sqrt{2}}{2} l K_l \\ -\frac{\sqrt{2}}{2} l K_l & \frac{\sqrt{2}}{2} l K_l & \frac{\sqrt{2}}{2} l K_l & -\frac{\sqrt{2}}{2} l K_l \\ -\zeta & \zeta & -\zeta & \zeta \end{bmatrix} \begin{bmatrix} w_1^2 \\ w_2^2 \\ w_3^2 \\ w_4^2 \end{bmatrix}. \quad (4)$$

Here, K_l is the lift coefficient, l denotes the distance between a rotor and the center of mass of the quadrotor, and ζ represents the reverse moment coefficient.

Let $u_1 = (s_\phi s_\psi + c_\phi s_\theta c_\psi) u_3$ and $u_2 = (-s_\phi c_\psi + c_\phi s_\theta s_\psi) u_3$ represent the virtual control inputs to cope with the under-actuation property. Then, the dynamical equations subjected to external disturbance can be further transformed into the following form:

$$\begin{cases} \dot{\Gamma}_1(t) = \Gamma_2(t), \\ \dot{\Gamma}_2(t) = \mathcal{Q}(\Gamma_2(t)) + \mathcal{G}(\Gamma_1(t)) \mathbf{u}(t) + \boldsymbol{\delta}(t), \end{cases} \quad (5)$$

where $\boldsymbol{\delta}(t) \in \mathbb{R}^6$ signifies the bounded disturbance; $\mathbf{u}(t) = [u_1, u_2, u_3, u_4, u_5, u_6]^T$ denotes the control input; $\Gamma_1(t) = [x, y, z, \phi, \theta, \psi]^T$ refers to the actual position and attitude; and $\mathcal{Q}(\Gamma_2(t))$ and $\mathcal{G}(\Gamma_1(t))$ are represented by

$$\mathcal{Q}(\Gamma_2(t)) = \begin{bmatrix} -K_{dx}\dot{x}/m \\ -K_{dy}\dot{y}/m \\ -K_{dz}\dot{z}/m - g \\ (J_y - J_z) \dot{\theta} \dot{\psi} / J_x - J_r \bar{\Omega} \dot{\theta} / J_x - K_{fx} \dot{\phi} / J_x \\ (J_z - J_x) \dot{\phi} \dot{\psi} / J_x + J_r \bar{\Omega} \dot{\phi} / J_x - K_{fy} \dot{\theta} / J_y \\ (J_x - J_y) \dot{\phi} \dot{\theta} / J_z - K_{fz} \dot{\psi} / J_z \end{bmatrix},$$

$$\mathcal{G}(\Gamma_1(t)) = \text{diag}(1/m, 1/m, c_\phi c_\theta / m, 1/J_x, 1/J_y, 1/J_z).$$

Then, define the following tracking error to monitor the tracking process:

$$\boldsymbol{\varepsilon}(t) = \Gamma_1(t) - \Gamma_d(t), \quad (6)$$

where $\Gamma_d(t) = [x_d, y_d, z_d, \phi_d, \theta_d, \psi_d]^T \in \mathbb{R}^6$ denotes a differentiable reference position and attitude. To this end, the tracking error system is obtained as follows:

$$\begin{cases} \dot{\boldsymbol{\varepsilon}}(t) = \dot{\Gamma}_1(t) - \dot{\Gamma}_d(t) \\ \ddot{\boldsymbol{\varepsilon}}(t) = \mathcal{Q}(\Gamma_2(t)) + \mathcal{G}(\Gamma_1(t)) \mathbf{u}(t) - \ddot{\Gamma}_d(t) + \boldsymbol{\delta}(t). \end{cases} \quad (7)$$

III. ADAPTIVE ROBUST PREDEFINED-TIME NONSINGULAR SMC

This section introduces two ZNN schemes and a novel AF by integrating a dynamic adaptive parameter and a fuzzy adaptive parameter, including a predefined-time AF (PTAF). The fuzzy adaptive parameter, derived from the Takagi-Sugeno fuzzy logic system (TSFSL), is tailored to enhance robustness and minimize chattering. The section also details the design of the TSFSL's fuzzy inference with two rule bases, each containing twelve rules, for adaptive error correction. Finally, it presents the ARPTNSMC scheme based on the two ZNN schemes, two adaptive parameters, and AFs.

A. Evolution Laws of ZNN and UZNN

We are now in a position to introduce two ZNN schemes that will serve as the basis for the novel SMC scheme, such that $\boldsymbol{\varepsilon}(t)$ can converge to zero in fixed/predefined-time through exploiting an appropriate AF [23], [24]. According to Refs. [23], [24], [42], the evolution laws of the general ZNN and the unified ZNN (UZNN) are formulated as follows:

$$\dot{\boldsymbol{\xi}}(t) = -\eta_1 \mathcal{P}(\boldsymbol{\xi}(t)), \quad (8)$$

$$\dot{\boldsymbol{\xi}}(t) = -\eta_1 \mathcal{P}(\boldsymbol{\xi}(t)) - \eta_2 \mathcal{P} \left(\boldsymbol{\xi}(t) + \int_0^t \eta_1 \mathcal{P}(\boldsymbol{\xi}(\tau)) d\tau \right), \quad (9)$$

where $\boldsymbol{\xi}(t) \in \mathbb{R}^n$ denotes the state variable; $\eta_1 > 0$ and $\eta_2 > 0$ are fixed parameters; and $\mathcal{P}(\cdot) : \mathbb{R}^n \rightarrow \mathbb{R}^n$ represents the AF array with its element being $p(\cdot) : \mathbb{R} \rightarrow \mathbb{R}$.

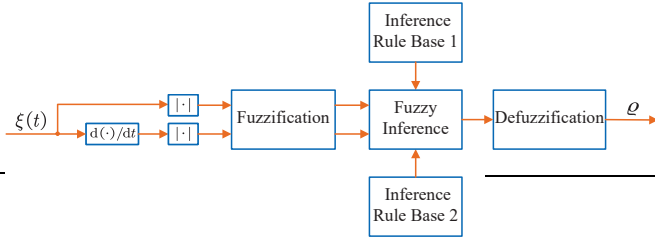


Fig. 1. Block diagram of the TSFLS.

B. Two Novel Activation Functions

Inspired by [31], [32], [43], two novel PTAFs are constructed to attain predefined-time property. The first AF $\mathcal{P}_1(\cdot)$ is a fuzzy adaptive PTAF with the element form denoted by

$$p_1(\xi) = \frac{4\lambda}{\mathcal{T}_p} (|\xi|^\alpha + |\xi|^\beta) \text{sign}(\xi) + \varrho \text{sign}(\xi) + \rho(\xi)\xi, \quad (10)$$

where \mathcal{T}_p is the predetermined parameter used to control the convergence time independently, $\alpha > 1$, $0 < \beta < 1$, and $\lambda = \pi \csc((1 - \beta)\pi/(\alpha - \beta))/(\alpha - \beta)$. Besides, $\varrho \geq 0$ denotes the fuzzy adaptive parameter generated by the TSFLS in Section III-C to enhance the robustness while suppressing the chattering caused by the discontinuous $\text{sign}(\xi)$, and $\rho(\xi)$ denotes the dynamic adaptive parameter with expression being

$$\rho(\xi) = \exp\left(\mu \text{arccsc}\left(\frac{1}{|\xi|} + 1\right)\right), \quad (11)$$

where $\mu > 0$, $\text{arccsc}(\cdot)$ denotes inverse cosecant function. The novel dynamic adaptive parameter (11) is designed to further enhance noise-tolerant performance.

The second AF, $\mathcal{P}_2(\cdot)$, is a differentiable PTAF with its element form $p_2(\cdot)$ defined by

$$p_2(\xi) = \begin{cases} \frac{2\lambda}{\mathcal{T}_p} (|\xi|^\alpha + |\xi|^\beta) \text{sign}(\xi), & \text{if } |\xi| > \epsilon_1, \\ \frac{2\lambda}{\mathcal{T}_p} (\iota_1 \xi + \iota_2 \xi^2 \text{sign}(\xi)), & \text{if } |\xi| \leq \epsilon_1, \end{cases} \quad (12)$$

where ϵ_1 is a small positive constant, $\iota_1 = (2 - \alpha)\epsilon_1^{\alpha-1} + (2 - \beta)\epsilon_1^{\beta-1}$, and $\iota_2 = (\alpha - 1)\epsilon_1^{\alpha-2} + (\beta - 1)\epsilon_1^{\beta-2}$.

The differentiable PTAF will be used to construct a sliding mode surface in the ZNN framework to ensure the predefined-time reachability of the sliding mode surface.

C. Takagi-Sugeno Fuzzy Logic System

Inspired by the adaptivity of the TSFLS [28], [44]–[47], we utilize a fuzzy adaptive gain (i.e. fuzzy adaptive parameter) to replace the constant gain in the discontinuous sign item, aimed at suppressing chattering. For this purpose, a TSFLS is presented, with the design process divided into fuzzification, fuzzy inference, and defuzzification. Besides, the block diagram of the TSFLS is displayed in Fig. 1.

Fuzzification: This step involves the mapping of accurate input values to fuzzy values through membership functions with the input values $\chi_1 = |\xi(t)|$ and $\chi_2 = |\dot{\xi}(t)|$. The Gaussian membership function is selected:

$$M(\chi) = \exp\left(-\frac{(\chi - o_1)^2}{2o_2^2}\right) \quad (13)$$

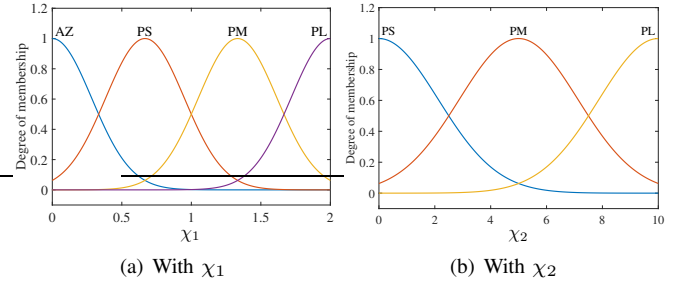


Fig. 2. Gaussian membership functions with input χ_1 and input χ_2 .

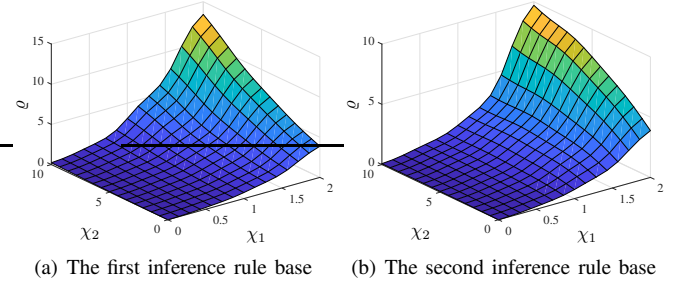


Fig. 3. Surfaces of the TSFLS utilizing two inference rule bases.

with constant parameters o_1 and o_2 . Besides, Gaussian membership functions corresponding to χ_1 and χ_2 are depicted in Fig. 2.

Fuzzy inference: In the fuzzy inference step, two inference rule bases are employed to better adapt to input changes, where each rule base includes twelve rules. If $\xi(t)\dot{\xi}(t) \geq 0$, the first inference rule base is selected, otherwise, the second inference rule base is employed.

The first inference rule base is as follows:

- R_1 : If χ_1 is PL and χ_2 is PL, then $\sigma_1 = 2\chi_1 + 1\chi_2$;
- R_2 : If χ_1 is PL and χ_2 is PM, then $\sigma_2 = 2\chi_1 + 0.8\chi_2$;
- R_3 : If χ_1 is PL and χ_2 is PS, then $\sigma_3 = 2\chi_1 + 0.6\chi_2$;
- R_4 : If χ_1 is PM and χ_2 is PL, then $\sigma_4 = 1\chi_1 + 0.4\chi_2$;
- R_5 : If χ_1 is PM and χ_2 is PM, then $\sigma_5 = 1\chi_1 + 0.2\chi_2$;
- R_6 : If χ_1 is PM and χ_2 is PS, then $\sigma_6 = 1\chi_1 + 0.1\chi_2$;
- R_7 : If χ_1 is PS and χ_2 is PL, then $\sigma_7 = 0.5\chi_1 + 0.08\chi_2$;
- R_8 : If χ_1 is PS and χ_2 is PM, then $\sigma_8 = 0.5\chi_1 + 0.06\chi_2$;
- R_9 : If χ_1 is PS and χ_2 is PS, then $\sigma_9 = 0.5\chi_1 + 0.04\chi_2$;
- R_{10} : If χ_1 is AZ and χ_2 is PL, then $\sigma_{10} = 0.2\chi_1 + 0.02\chi_2$;
- R_{11} : If χ_1 is AZ and χ_2 is PM, then $\sigma_{11} = 0.2\chi_1 + 0.01\chi_2$;
- R_{12} : If χ_1 is AZ and χ_2 is PS, then $\sigma_{12} = 0.2\chi_1 + 0.005\chi_2$.

The second inference rule base is provided as follows:

- R_1 : If χ_1 is PL and χ_2 is PL, then $\sigma_1 = 2\chi_1 + 0.6\chi_2$;
- R_2 : If χ_1 is PL and χ_2 is PM, then $\sigma_2 = 2\chi_1 + 0.8\chi_2$;
- R_3 : If χ_1 is PL and χ_2 is PS, then $\sigma_3 = 2\chi_1 + 1\chi_2$;
- R_4 : If χ_1 is PM and χ_2 is PL, then $\sigma_4 = 1\chi_1 + 0.1\chi_2$;
- R_5 : If χ_1 is PM and χ_2 is PM, then $\sigma_5 = 1\chi_1 + 0.2\chi_2$;
- R_6 : If χ_1 is PM and χ_2 is PS, then $\sigma_6 = 1\chi_1 + 0.4\chi_2$;
- R_7 : If χ_1 is PS and χ_2 is PL, then $\sigma_7 = 0.5\chi_1 + 0.04\chi_2$;
- R_8 : If χ_1 is PS and χ_2 is PM, then $\sigma_8 = 0.5\chi_1 + 0.06\chi_2$;
- R_9 : If χ_1 is PS and χ_2 is PS, then $\sigma_9 = 0.5\chi_1 + 0.08\chi_2$;
- R_{10} : If χ_1 is AZ and χ_2 is PL, then $\sigma_{10} = 0.2\chi_1 + 0.005\chi_2$;
- R_{11} : If χ_1 is AZ and χ_2 is PM, then $\sigma_{11} = 0.2\chi_1 + 0.01\chi_2$;
- R_{12} : If χ_1 is AZ and χ_2 is PS, then $\sigma_{12} = 0.2\chi_1 + 0.02\chi_2$;

where the fuzzy sets PL, PM, PS, and AZ denote positive large, positive medium, positive small, and almost zero, respectively.

Defuzzification: The function of defuzzification is to convert fuzzy variables in the TSFLS into a precise value. The wtaver method [28] in this process is considered as follows:

$$\varrho = \frac{\sum_{q=1}^{12} \varsigma_q \sigma_q}{\sum_{q=1}^{12} \varsigma_q}$$

with $\varsigma_q = M_q(\chi_1)M_q(\chi_2)$ being the weight of the output σ_q of the q -th rule in the total output, where $M_q(\chi_1)$ and $M_q(\chi_2)$ represent degree of membership of χ_1 and χ_2 in the q -th rule belonging to the fuzzy set.

Finally, the surfaces of the TSFLS utilizing two inference rule bases are exhibited in Fig. 3. The results indicate that the output ϱ will change adaptively with two inputs $\chi_1 = |\xi(t)|$ and $\chi_2 = |\dot{\xi}(t)|$.

D. Sliding Mode Surface Based on ZNN

Firstly, considering differentiable PTAF (12) and the input $\varepsilon(t)$, we rewrite the evolution law (8) with $\eta_1 = 1$ as

$$\dot{\varepsilon}(t) = -\mathcal{P}_2(\varepsilon(t)). \quad (14)$$

Then, shifting the right-hand side of (14) to the left-hand side, the state variable of nonsingular sliding mode surface (SMS) based on the ZNN is obtained as

$$s(t) = \dot{\varepsilon}(t) + \mathcal{P}_2(\varepsilon(t)) \quad (15)$$

with its derivative being

$$\dot{s}(t) = \ddot{\varepsilon}(t) + \frac{\partial \mathcal{P}_2(\varepsilon(t))}{\partial \varepsilon} \dot{\varepsilon}(t). \quad (16)$$

Remark 1. Note that the dynamic properties of the SMS constructed by ZNN depend on the evolution law and differentiable AF of ZNN. Following the design framework of (14) and (15), SMSs with different properties can be simply constructed by utilizing the existing finite-time, fixed-time, and predefined-time convergent ZNN approaches. Therefore, compared with traditional SMS, the method of constructing SMS using ZNN has two main advantages: 1) it is simpler and clearer because it follows a fixed design framework; 2) it realizes the predefined-time reachability of the nonsingularity SMS due to the differentiable PTAF designed under the framework of ZNN.

E. Controller Based on Fuzzy Neural Network

In order to make $\varepsilon(t)$ reach SMS (15), an approaching law is put forward by utilizing fuzzy neural network (i.e., evolution law (9) with $\eta_1 = \eta_2 = 1$ and fuzzy adaptive PTAF (10)):

$$\dot{s}(t) = -\mathcal{P}_1(s(t)) - \mathcal{P}_1\left(s(t) + \int_0^t \mathcal{P}_1(s(\tau))d\tau\right). \quad (17)$$

Then, combining (7), (16), and (17), the adaptive robust predefined-time nonsingular controller (dependent on the fuzzy neural network) is developed:

$$u(t) = \mathcal{G}^{-1}(\Gamma_1(t)) \left(-\frac{\partial \mathcal{P}_2(\varepsilon(t))}{\partial \varepsilon} (\dot{\Gamma}_1(t) - \dot{\Gamma}_d(t)) - \mathcal{P}_1(s(t)) - \mathcal{Q}(\Gamma_2(t)) + \ddot{\Gamma}_d(t) - \mathcal{P}_1\left(s(t) + \int_0^t \mathcal{P}_1(s(\tau))d\tau\right) \right). \quad (18)$$

IV. THEORETICAL ANALYSIS

This section establishes the predefined-time reachability of SMS (15), along with the predefined-time convergence and robustness of the closed-loop system. Note that the initial state is represented by $\Gamma_0 = [\Gamma_1^T(0), \Gamma_2^T(0)]^T$ in the following analysis.

Theorem 1. Consider a differentiable reference trajectory $\Gamma_d(t)$. For external disturbance $\delta(t) = \mathbf{0}$ and randomly generated initial state Γ_0 , the tracking error $\varepsilon(t)$ of the system (5) by applying the controller (18) can move to SMS (15) within predefined-time $\mathcal{T}_p/2$, where \mathcal{T}_p is the predetermined parameter from PTAF (10).

Proof: Firstly, substituting the controller (18) into the error system (7) yields

$$\ddot{\varepsilon}(t) = -\frac{\partial \mathcal{P}_2(\varepsilon(t))}{\partial \varepsilon} \dot{\varepsilon}(t) - \mathcal{P}_1(s(t)) - \mathcal{P}_1\left(s(t) + \int_0^t \mathcal{P}_1(s(\tau))d\tau\right) + \delta(t). \quad (19)$$

According to (16), (19) is transformed into

$$\dot{s}(t) = -\mathcal{P}_1(s(t)) - \mathcal{P}_1\left(s(t) + \int_0^t \mathcal{P}_1(s(\tau))d\tau\right) + \delta(t). \quad (20)$$

Since disturbance $\delta(t) = \mathbf{0}$, (20) is written as

$$\dot{s}(t) = -\mathcal{P}_1(s(t)) - \mathcal{P}_1\left(s(t) + \int_0^t \mathcal{P}_1(s(\tau))d\tau\right). \quad (21)$$

Define an auxiliary variable

$$v(t) = s(t) + \int_0^t \mathcal{P}_1(s(\tau))d\tau. \quad (22)$$

Then, we obtain

$$\dot{v}(t) = \dot{s}(t) + \mathcal{P}_1(s(t)) = -\mathcal{P}_1(v(t)) \quad (23)$$

with element being $\dot{v}(t) = -p_1(v_j(t))$, where $v_j(t)$ is the j -th element of $v(t)$.

Denoting $\varpi_1(t) = v^T(t)v(t)$ as a Lyapunov function, we have

$$\begin{aligned} \dot{\varpi}_1(t) &= 2 \sum_{j=1}^6 v_j(t) \dot{v}_j(t) \\ &= -2 \sum_{j=1}^6 v_j(t) p_1(v_j(t)) \leq 0 \end{aligned}$$

because $p_1(\cdot)$ is a monotonically increasing odd function. Thus, (23) is globally asymptotically stable in the Lyapunov sense. With the fact of $v_j(T(v_j(0))) = 0$, which is a direct

corollary of Definition 1, it is not difficult to obtain the settling time of system (23) as follows:

$$\begin{aligned}
 T(v_j(0)) &= \int_0^{T(v_j(0))} dt \\
 &= \int_{v_j(T(v_j(0)))}^{v_j(0)} \frac{1}{p_1(v_j)} dv_j \\
 &= \int_0^{|v_j(0)|} \frac{1}{\frac{4\lambda}{T_p} (v_j^\alpha + v_j^\beta) + \varrho + \rho(v_j)v_j} dv_j \\
 &\leq \frac{T_p}{4\lambda} \int_0^{+\infty} \frac{1}{v_j^\alpha + v_j^\beta} dv_j.
 \end{aligned} \tag{24}$$

Denoting

$$\varphi = \frac{1}{v_j^{\alpha-\beta} + 1} = \frac{v_j^\beta}{v_j^\alpha + v_j^\beta},$$

we have

$$\begin{cases} v_j = (1/\varphi - 1)^{\frac{1}{\alpha-\beta}}, \\ dv_j = -\frac{(1-\varphi)^{-1+\frac{1}{\alpha-\beta}}}{(\alpha-\beta)\varphi^{1+\frac{1}{\alpha-\beta}}} d\varphi. \end{cases}$$

In the light of $\lambda = \pi \csc((1-\beta)\pi/(\alpha-\beta))/(\alpha-\beta)$, Definition 5, and Lemma 1, an upper bound of settling time can be calculated by

$$\begin{aligned}
 T(v(0)) &\leq \frac{T_p}{4\lambda} \int_0^{+\infty} \frac{1}{v_j^\alpha + v_j^\beta} dv_j \\
 &= \frac{-T_p}{4\lambda(\alpha-\beta)} \int_1^0 \varphi^{\frac{\beta-1}{\alpha-\beta}} (1-\varphi)^{\frac{1-\beta}{\alpha-\beta}-1} d\varphi \\
 &= \frac{T_p}{4\lambda(\alpha-\beta)} B\left(1 - \frac{1-\beta}{\alpha-\beta}, \frac{1-\beta}{\alpha-\beta}\right) \\
 &= \frac{\pi T_p}{4\lambda(\alpha-\beta)} \csc\left(\frac{1-\beta}{\alpha-\beta}\pi\right) \\
 &= \frac{T_p}{4}.
 \end{aligned} \tag{25}$$

Therefore, the system (21) evolves over time as

$$\dot{s}(t) = -\mathcal{P}_1(s(t)), t \geq T_p/4. \tag{26}$$

Since system (26) shares the same expression as system (23), the settling time of system (26) is calculated by

$$T(s(T_p/4)) \leq T_p/4.$$

Finally, we can obtain the total convergence time T_{c1} satisfying

$$T_{c1} = T(v(0)) + T(s(T_p/4)) \leq T_p/2.$$

As a result, the sliding variable $s(t)$ converges to zero within time $T_p/2$, i.e., the tracking error $\varepsilon(t)$ of the system (5) utilizing the controller (18) can move to SMS (15) within a predefined-time $T_p/2$, which ends the proof. ■

Theorem 2. Consider a differentiable reference trajectory $\Gamma_d(t)$. For disturbance $\delta(t) = \mathbf{0}$ and randomly generated initial state Γ_0 , the tracking error of the system (5) applying the controller (18) can converge to the following band

$$|\varepsilon_j(t)| \leq \epsilon_1, j \in \{1, 2, \dots, 6\}$$

within predefined-time T_p , where ϵ_1 is a small positive constant.

Proof: Firstly, the sliding variable $s(t)$ can be stabilized to zero within predefined-time $T_p/2$ if $\delta(t) = \mathbf{0}$ according to Theorem 1, indicating that $s(t) = \dot{s}(t) = \mathbf{0}$ for any $t \geq T_p/2$. From (15), we deduce that

$$\dot{\varepsilon}(t) = -\mathcal{P}_2(\varepsilon(t)), \forall t \in [T_p/2, +\infty), \tag{27}$$

where its element is $\dot{\varepsilon}_j(t) = -p_2(\varepsilon_j(t))$. Likewise, defining a Lyapunov function

$$\varpi_2(t) = \varepsilon_j^2(t) \tag{28}$$

and differentiating it with respect to t lead to

$$\begin{aligned} \dot{\varpi}_2(t) &= 2\varepsilon_j(t)\dot{\varepsilon}_j(t) \\ &= -2\varepsilon_j(t)p_2(\varepsilon_j(t)) \leq 0 \end{aligned}$$

due to the fact that $p_2(\cdot)$ defined in (12) is a monotonically increasing odd function. Therefore, on the basis of the Lyapunov stability theory, the system (27) is globally asymptotically stable. Thus, we can assume that $|\varepsilon_j(t)|$ approaches ϵ_1 within time T_{ce1} , that is, $\varepsilon_j(T_p/2 + T_{ce1}) = \epsilon_1$. Moreover, according to (24) and (25), if $|\varepsilon_j(T_p/2)| > \epsilon_1$, the time T_{ce1} is estimated by

$$\begin{aligned}
 T_{ce1} &= \int_{T_p/2}^{T_p/2+T_{ce1}} dt \\
 &= \int_{\epsilon_1}^{|\varepsilon_j(T_p/2)|} \frac{1}{p_2(\varepsilon_j)} d\varepsilon_j \\
 &< \frac{T_p}{2\lambda} \int_0^{+\infty} \frac{1}{\varepsilon_j^\alpha + \varepsilon_j^\beta} d\varepsilon_j \\
 &= \frac{T_p}{2}.
 \end{aligned} \tag{29}$$

Then, we obtain the time T_{c2} for $|\varepsilon_j(t)|$ to converge from $|\varepsilon_j(0)|$ to ϵ_1 as follows:

$$T_{c2} = T_p/2 + T_{ce1} < T_p.$$

Accordingly, the tracking error $\varepsilon(t)$ of the system (5) utilizing the controller (18) approaches ϵ_1 within predefined-time T_p , and the proof is now complete. ■

Theorem 3. Consider a differentiable reference trajectory $\Gamma_d(t)$. If each element in disturbance vector $\delta(t)$ is bounded by $|\delta_j(t)| \leq \varrho + \rho(v_j(t))|v_j(t)|$, for randomly generated initial state Γ_0 , the tracking error of the system (5) applying the controller (18) can converge to the following band

$$|\varepsilon_j(t)| \leq \epsilon_1, j \in \{1, 2, \dots, 6\}$$

within predefined-time T_p , where ϵ_1 is a small positive constant.

Proof: The j -th subsystem of (20) is obtained:

$$\dot{s}_j(t) = -p_1(s_j(t)) - p_1\left(s_j(t) + \int_0^t p_1(s_j(\tau))d\tau\right) + \delta_j(t). \tag{30}$$

Considering the element of the auxiliary variable (22) is $v_j(t) = s_j(t) + \int_0^t p_1(s_j(\tau))d\tau$, $\dot{v}_j(t)$ is calculated by

$$\dot{v}_j(t) = -p_1(v_j(t)) + \delta_j(t). \tag{31}$$

A Lyapunov function is defined by

$$\varpi_3(t) = v_j^2(t). \quad (32)$$

Due to $|\delta_j(t)| \leq \varrho + \rho(v_j(t))|v_j(t)|$, we have

$$\begin{aligned} \dot{\varpi}_3(t) &= 2v_j(t)\dot{v}_j(t) \\ &= 2v_j(t)(-p_1(v_j(t)) + \delta_j(t)) \\ &\leq -\frac{8\lambda}{\mathcal{T}_p} (|v_j(t)|^{\alpha+1} + |v_j(t)|^{\beta+1}) - 2\varrho|v_j(t)| \\ &\quad - 2\rho(v_j(t))|v_j(t)|^2 + 2|v_j(t)||\delta_j(t)| \\ &\leq -\frac{8\lambda}{\mathcal{T}_p} \left(\varpi_3^{\frac{\alpha+1}{2}}(t) + \varpi_3^{\frac{\beta+1}{2}}(t) \right). \end{aligned} \quad (33)$$

Furthermore, it follows from (33) that

$$dt \leq -\frac{\mathcal{T}_p}{8\lambda \left(\varpi_3^{\frac{\alpha+1}{2}}(t) + \varpi_3^{\frac{\beta+1}{2}}(t) \right)} d\varpi_3. \quad (34)$$

Similar to (25), by integrating both sides of (34) from 0 to $T(\varpi_3(0))$ with respect to the time variable t , the settling time of $\varpi_3(t)$ is calculated as follows:

$$\begin{aligned} T(\varpi_3(0)) &\leq \frac{\mathcal{T}_p}{8\lambda} \int_{\varpi_3(0)}^0 -\frac{1}{\varpi_3^{\frac{\alpha+1}{2}}(t) + \varpi_3^{\frac{\beta+1}{2}}(t)} d\varpi_3 \\ &\leq \frac{\mathcal{T}_p}{8\lambda} \int_0^{+\infty} \frac{1}{\varpi_3^{\frac{\alpha+1}{2}}(t) + \varpi_3^{\frac{\beta+1}{2}}(t)} d\varpi_3 \\ &= \frac{\pi\mathcal{T}_p}{8\lambda \frac{(\alpha-\beta)}{2}} \csc\left(\frac{1-\beta}{\alpha-\beta}\pi\right) \\ &= \frac{\mathcal{T}_p}{4}. \end{aligned} \quad (35)$$

Therefore, the subsystem (30) evolves over time to

$$\dot{s}_j(t) = -p_1(s_j(t)), t \geq \mathcal{T}_p/4. \quad (36)$$

Based on the system (26), the settling time of the subsystem (36) is calculated as $T(s_j(\mathcal{T}_p/4)) \leq \mathcal{T}_p/4$. Thus, from (15), we deduce that the j -th subsystem satisfies

$$\dot{\varepsilon}_j(t) = -p_2(\varepsilon_j(t)), \forall t \in [\mathcal{T}_p/2, +\infty). \quad (37)$$

Based on (27)-(29) in Theorem 2, the time T_{ce2} for $|\varepsilon_j(t)|$ to converge from $|\varepsilon_j(\mathcal{T}_p/2)|$ to ε_1 satisfying $T_{ce2} < \mathcal{T}_p/2$ can be inferred.

Finally, the time T_{c3} for $|\varepsilon_j(t)|$ to converge from $|\varepsilon_j(0)|$ to ε_1 is obtained by

$$T_{c3} = T(\varpi_3(0)) + T(s_j(\mathcal{T}_p/4)) + T_{ce2} < \mathcal{T}_p,$$

and the proof is now complete. ■

Theorem 4. Consider a differentiable reference trajectory $\Gamma_d(t)$. If each element in disturbance vector $\delta(t)$ is bounded by $|\delta_j(t)| \leq \delta_{max}$, for randomly generated initial state Γ_0 , the tracking error of the system (5) applying the controller (18) can converge to the following band

$$|\varepsilon_j(t)| \leq \frac{\mathcal{T}_p^2 \delta_{max}}{4\lambda^2 + \lambda\mathcal{T}_p}, j \in \{1, 2, \dots, 6\},$$

where δ_{max} is a constant.

Proof: Following $\varpi_3(t)$ in (32), we obtain

$$\begin{aligned} \dot{\varpi}_3(t) &= 2v_j(t)\dot{v}_j(t) \\ &= 2v_j(t)(-p_1(v_j(t)) + \delta_j(t)) \\ &\leq 2|v_j(t)|(-|p_1(v_j(t))| + |\delta_j(t)|) \\ &\leq 2|v_j(t)|(-|p_1(v_j(t))| + \delta_{max}). \end{aligned} \quad (38)$$

From (38), we can infer that $|p_1(v_j(t))| \leq \delta_{max}$ as $t \rightarrow \infty$.

Analogously, denote a Lyapunov function $\varpi_4(t) = s_j^2(t)$. It follows from (30) that

$$\begin{aligned} \dot{\varpi}_4(t) &= 2s_j(t)\dot{s}_j(t) \\ &= 2s_j(t)(-p_1(s_j(t)) - p_1(v_j(t)) + \delta_j(t)) \\ &\leq 2|s_j(t)|(-|p_1(s_j(t))| + |p_1(v_j(t))| + |\delta_j(t)|) \\ &\leq 2|s_j(t)|(-|p_1(s_j(t))| + 2\delta_{max}) \end{aligned}$$

as $t \rightarrow \infty$. Consequently, $s_j(t)$ converges to the band of $|s_j(t)| \leq |p_1^{-1}(2\delta_{max})|$ as $t \rightarrow \infty$, where $p_1^{-1}(\cdot)$ is the inverse function of $p_1(\cdot)$. Moreover, $|p_1(\xi)| \geq |(4\lambda/\mathcal{T}_p + \rho(\xi))\xi|$ keeps correct from (10), then $|p_1^{-1}(\xi)| \leq |\xi/(4\lambda/\mathcal{T}_p + \rho(\xi))|$ is obtained. Thus, $s_j(t)$ can converge to the band of $|s_j(t)| \leq 2\delta_{max}/(4\lambda/\mathcal{T}_p + \rho(s_j(t)))$.

According to (15), we know $\dot{\varepsilon}_j(t) = -p_2(\varepsilon_j(t)) + s_j(t)$. Furthermore, as $t \rightarrow \infty$, it follows from (28) that

$$\begin{aligned} \dot{\varpi}_2(t) &= 2\varepsilon_j(t)\dot{\varepsilon}_j(t) \\ &= 2\varepsilon_j(t)(-p_2(\varepsilon_j(t)) + s_j(t)) \\ &\leq 2|\varepsilon_j(t)|(-|p_2(\varepsilon_j(t))| + |s_j(t)|) \\ &\leq 2|\varepsilon_j(t)| \left(-|p_2(\varepsilon_j(t))| + \frac{2\delta_{max}}{4\lambda/\mathcal{T}_p + \rho(s_j(t))} \right). \end{aligned}$$

Hence, $\varepsilon_j(t)$ can converge to the band of $|\varepsilon_j(t)| \leq |p_2^{-1}(2\delta_{max}/(4\lambda/\mathcal{T}_p + \rho(s_j(t))))|$. Besides, $|p_2^{-1}(\xi)| \leq |\mathcal{T}_p\xi/(2\lambda)|$ is obtained due to the fact that $|p_2(\xi)| \geq |2\lambda\xi/\mathcal{T}_p|$ from (12). Therefore, as $t \rightarrow \infty$, the bound of $|\varepsilon_j(t)|$ can be written as

$$\begin{aligned} |\varepsilon_j(t)| &\leq \left| p_2^{-1} \left(\frac{2\delta_{max}}{4\lambda/\mathcal{T}_p + \rho(s_j(t))} \right) \right| \\ &\leq \frac{\mathcal{T}_p^2 \delta_{max}}{4\lambda^2 + \lambda\rho(s_j(t))\mathcal{T}_p} \\ &\leq \frac{\mathcal{T}_p^2 \delta_{max}}{4\lambda^2 + \lambda\mathcal{T}_p}, \end{aligned}$$

and the whole proof is over. ■

Remark 2. So far, a novel ARPTNSMC scheme has been developed to target fast and accurate tracking of a quadrotor under external disturbances. This scheme is based on a fuzzy neural network by combining fuzzy logic with a ZNN, and therefore stands out from traditional SMC methods in that a general ZNN and a differentiable predefined-time activation function are developed to form a nonsingular sliding mode surface. The control law includes both dynamic and fuzzy adaptive parameters, which are developed from the Takagi-Sugeno fuzzy logic system, to enhance robustness and reduce chattering. In Theorems 1-3, theoretical validation of the system's predefined-time convergence and robustness has

TABLE II
QUADROTOR PARAMETERS.

| Symbol | Value | Symbol | Value |
|----------|---------------------------------------------------------------------|---------|-----------------------------------------------------------------------|
| K_{fx} | $5.6 \times 10^{-4} \text{ N} \cdot \text{m}/(\text{rad}/\text{s})$ | m | 0.12 kg |
| K_{fy} | $5.6 \times 10^{-4} \text{ N} \cdot \text{m}/(\text{rad}/\text{s})$ | l | 0.13 m |
| K_{fz} | $6.4 \times 10^{-4} \text{ N} \cdot \text{m}/(\text{rad}/\text{s})$ | J_x | $6.7 \times 10^{-5} \text{ kg} \cdot \text{m}^2$ |
| K_{dx} | $5.6 \times 10^{-4} \text{ N}/(\text{m}/\text{s})$ | J_y | $7.5 \times 10^{-3} \text{ kg} \cdot \text{m}^2$ |
| K_{dy} | $5.6 \times 10^{-4} \text{ N}/(\text{m}/\text{s})$ | J_z | $7.5 \times 10^{-3} \text{ kg} \cdot \text{m}^2$ |
| K_{dz} | $6.4 \times 10^{-4} \text{ N}/(\text{m}/\text{s})$ | ζ | $3.2 \times 10^{-2} \text{ N} \cdot \text{m}/(\text{rad}/\text{s})^2$ |
| K_l | $3.0 \times 10^{-3} \text{ N}/(\text{rad}/\text{s})^2$ | J_r | $2.8 \times 10^{-5} \text{ N} \cdot \text{m}/(\text{rad}^2/\text{s})$ |

been provided. A practical example of butterfly-shaped trajectory tracking has been used to demonstrate the ARPTNSMC scheme's effectiveness.

Remark 3. In comparison to existing research results, this paper makes several distinct contributions as summarized below.

- 1) *Innovative Control Scheme:* A novel ARPTNSMC scheme is developed to enhance the tracking control performance of quadrotors especially under external disturbances.
- 2) *Fusion of Techniques:* The developed scheme uniquely combines fuzzy logic and ZNN to form a fuzzy neural network, which differs from traditional SMC methods. This integration provides a more robust and efficient control strategy.
- 3) *Advanced Activation Functions:* The paper proposes the use of a general ZNN and a differentiable predefined-time activation function to create a nonsingular sliding mode surface, which is a notable advancement over standard SMC approaches.
- 4) *Adaptive Parameters for Disturbance Compensation:* The introduction of both dynamic and fuzzy adaptive parameters in the control law is a key differentiator. The fuzzy adaptive parameter, derived from the Takagi-Sugeno fuzzy logic system, specifically targets the enhancement of robustness and the mitigation of chattering, which is a common issue in control systems.
- 5) *Theoretical and Practical Validation:* The paper provides theoretical proofs to validate the predefined-time convergence and robustness of the ARPTNSMC scheme. Furthermore, it substantiates these claims with a practical example of butterfly-shaped trajectory tracking, demonstrating the scheme's superior performance in convergence, robustness, and chattering suppression compared to existing methods.

In summary, the paper contributes a sophisticated, theoretically sound, and practically validated control scheme that advances the capabilities of quadrotor control systems in challenging environments.

V. ILLUSTRATION EXAMPLE

This section presents two illustrative examples using a quadrotor to validate the effectiveness of the ARPTNSMC scheme, with quadrotor parameters detailed in Table II. It

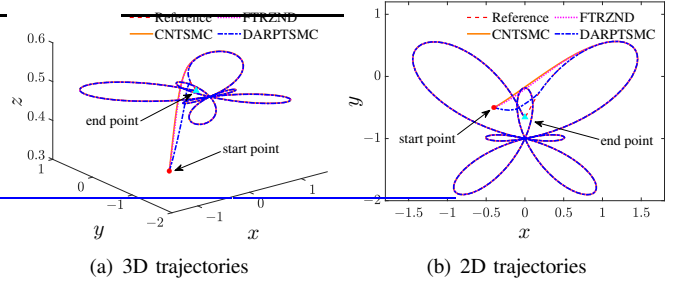


Fig. 4. Butterfly-shaped trajectories of the quadrotor controlled by three schemes when $\delta_j(t) = 0$.

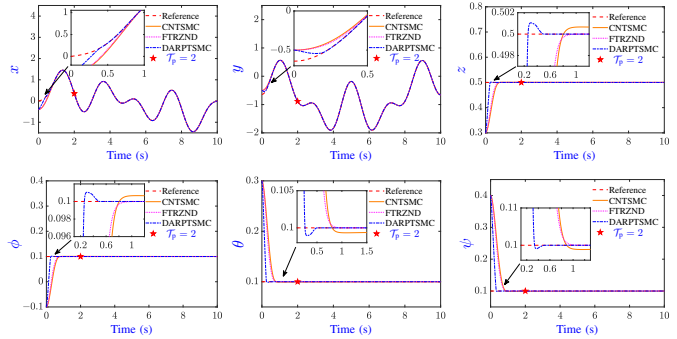


Fig. 5. States of the quadrotor controlled by three schemes when $\delta_j(t) = 0$.

also introduces the continuous nonsingular terminal SMC (CNTSMC) [33] and fixed-time robust ZNN (FTRZNN) [34] for comparative analysis, highlighting the advantages of the ARPTNSMC scheme.

A. Controllers for Comparison

To unify the SMC and ZNN schemes for comparison, the sliding variable is chosen as follows [31], [32]:

$$\mathbf{s}(t) = \dot{\boldsymbol{\varepsilon}}(t) + \eta_3 \mathcal{P}_3(\boldsymbol{\varepsilon}(t)), \quad (39)$$

where $\mathcal{P}_3(\cdot) : \mathbb{R}^n \rightarrow \mathbb{R}^n$ is a nonlinear vector function with element $p_3(\cdot) : \mathbb{R} \rightarrow \mathbb{R}$ being

$$p(\boldsymbol{\varepsilon}(t)) = \begin{cases} \boldsymbol{\varepsilon}^{c_1/c_2}(t), & \text{if } |\boldsymbol{\varepsilon}(t)| > \epsilon_2, \\ \boldsymbol{\varepsilon}^{c_1/c_2}(t) + \boldsymbol{\varepsilon}^2(t) \text{sign}(\boldsymbol{\varepsilon}(t)), & \text{if } |\boldsymbol{\varepsilon}(t)| \leq \epsilon_2, \end{cases}$$

where c_1 and c_2 are positive odd integers such that $0 < c_1/c_2 < 1$, $\boldsymbol{\varepsilon}^2 = (2 - c_1/c_2)\boldsymbol{\varepsilon}^{c_1/c_2-1}$, and $\boldsymbol{\varepsilon}^2 = (c_1/c_2 - 1)\boldsymbol{\varepsilon}^{c_1/c_2-2}$.

Next, the approaching law of the CNTSMC [33] and the evolution law of the FTRZNN [34] are

$$\begin{aligned} \dot{\mathbf{s}}(t) = & -k_1 |\mathbf{s}(t)|^{1/2} \text{sign}(\mathbf{s}(t)) - k_2 \mathbf{s}(t) \\ & - \int_0^t (k_3 \text{sign}(\mathbf{s}(\tau)) + k_4 \mathbf{s}(\tau)) d\tau, \end{aligned}$$

$$\begin{aligned} \dot{\mathbf{s}}(t) = & \eta_4 \left(-k_5 \exp(|\mathbf{s}(t)|^{k_6}) |\mathbf{s}(t)|^\beta \text{sign}(\mathbf{s}(t)) \right. \\ & \left. - k_7 \mathbf{s}(t) - k_8 \text{sign}(\mathbf{s}(t)) \right), \end{aligned}$$

where $k_1, k_2, k_3, k_4, k_5, k_6$, and k_7 are positive parameters; and $k_8 \geq 0$, $\alpha > 1$, and $0 < \beta < 1$. Thus, for the CNTSMC

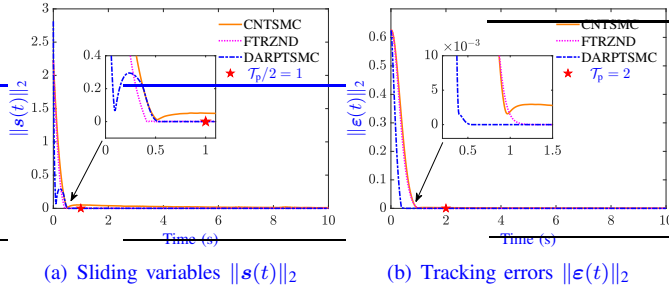


Fig. 6. Sliding variables $\|s(t)\|_2$ and tracking errors $\|\varepsilon(t)\|_2$ synthesized by three schemes when $\delta_j(t) = 0$.

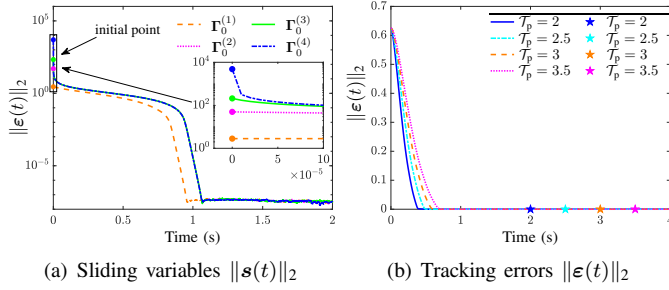


Fig. 7. Tracking errors $\|\varepsilon(t)\|_2$ synthesized by the ARPTNSMC scheme with various initial states Γ_0 and predetermined parameter values \mathcal{T}_p when $\delta_j(t) = 0$.

and the FTRZNN, controllers based on sliding variable (39) can be given, respectively, as follows:

$$\begin{aligned}
 \mathbf{u}(t) &= \mathcal{G}^{-1}(\Gamma_1(t)) \left(-\eta_3 \frac{\partial \mathcal{P}_3(\varepsilon(t))}{\partial \varepsilon} (\dot{\Gamma}_1(t) - \dot{\Gamma}_d(t)) \right. \\
 &\quad - \mathcal{Q}(\Gamma_2(t)) + \ddot{\Gamma}_d(t) - k_1 |s(t)|^{1/2} \text{sign}(s(t)) \\
 &\quad \left. - k_2 s(t) - \int_0^t (k_3 \text{sign}(s(\tau)) + k_4 s(\tau)) d\tau \right), \\
 \mathbf{u}(t) &= \mathcal{G}^{-1}(\Gamma_1(t)) \left(-\eta_3 \frac{\partial \mathcal{P}_3(\varepsilon(t))}{\partial \varepsilon} (\dot{\Gamma}_1(t) - \dot{\Gamma}_d(t)) \right. \\
 &\quad + \ddot{\Gamma}_d(t) - k_5 \exp(|s(t)|^{k_6}) |s(t)|^\beta \text{sign}(s(t)) \\
 &\quad \left. - k_7 s(t) - k_8 \text{sign}(s(t)) - \mathcal{Q}(\Gamma_2(t)) \right).
 \end{aligned}$$

Moreover, the parameters of (10)-(12) and the above controllers are set as $\mu = 16/\pi$; $\mathcal{T}_p = 2$, $\alpha = 2$, $\beta = 0.2$, $\epsilon_1 = \epsilon_2 = 0.01$; and $\eta_3 = 2$, $c_1 = 3$, $c_3 = 5$, $k_1 = k_2 = 2$, $\eta_4 = k_3 = k_4 = k_5 = k_7 = k_8 = 1$, $k_6 = 0.5$.

B. Butterfly-Shaped Trajectory

In this part, the objective is to track a given reference butterfly-shaped trajectory utilizing three control schemes. The reference trajectory is represented by

$$\begin{cases}
 x_d = 0.5 \sin(\pi t/5) \pi_1, \\
 y_d = -1 + 0.5 \cos(\pi t/5) \pi_1, \\
 z_d = 0.5,
 \end{cases}$$

and $\phi_d = \theta_d = \psi_d = 0.1$, where $\pi_1 = \exp(\cos(\pi t/5)) - 2 \cos(4\pi t/5) - \sin^5(\pi t/60)$. The initial state is $\Gamma_0 = [-0.4, 0, -0.5, 0, 0.3, 0, -0.1, 0, 0.3, 0, 0.4, 0]^T$.

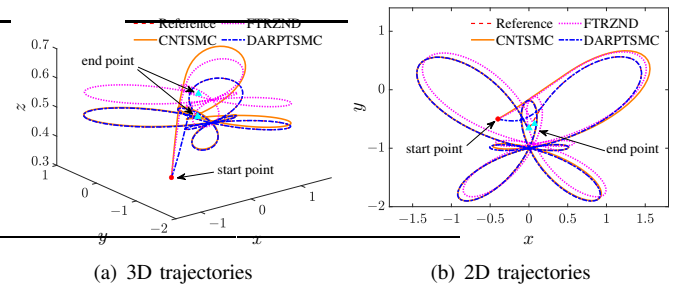


Fig. 8. Butterfly-shaped trajectories tracking of the quadrotor controlled by three schemes when $\delta_j(t) = 3$.

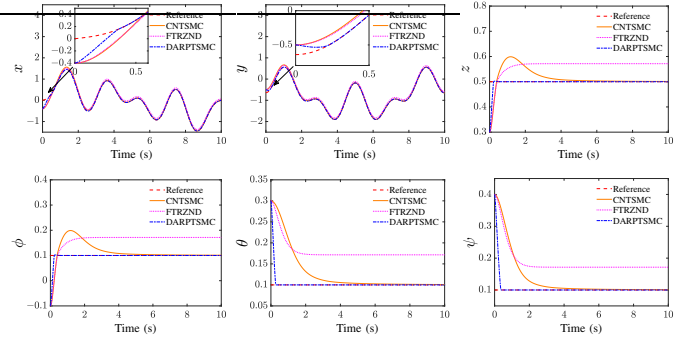


Fig. 9. States of the quadrotor controlled by three schemes when $\delta_j(t) = 3$.

1) *Convergence analysis*: In this part of the study, Fig. 4 depicts butterfly-shaped trajectories executed by three different control schemes, with red dotted lines indicating the reference trajectory. The ARPTNSMC scheme's performance, both in 3D and 2D trajectories as shown in Figs. 4(a) and 4(b), demonstrates a quicker convergence to the reference trajectory compared to the other schemes when disturbances $\delta_j(t) = 0$. Additionally, Fig. 5 displays the position and attitude outcomes for the quadrotor under the same three schemes without disturbances. The results clearly show that the ARPTNSMC scheme achieves a faster approach to the desired position and attitude of the quadrotor than the other two schemes. Furthermore, Fig. 6 presents the comparison of sliding variables $\|s(t)\|_2$ and tracking errors $\|\varepsilon(t)\|_2$ across these schemes. It's observed that while the convergence time of $\|s(t)\|_2$ is almost identical for the ARPTNSMC and FTRZNN schemes, the $\|\varepsilon(t)\|_2$ converges to zero more rapidly under the ARPTNSMC scheme. In summary, Figs. 4 to 6 collectively indicate that the closed-loop system controlled by the ARPTNSMC scheme achieves a faster convergence rate compared to the other two schemes.

In Fig. 7, the tracking errors $\|\varepsilon(t)\|_2$ according to the ARPTNSMC with various initial states Γ_0 and predetermined parameter values \mathcal{T}_p are exhibited. Furthermore, the p -th Γ_0 is represented by $\Gamma_0^{(p)}$ ($p \in \{1, 2, 3, 4\}$), where $\Gamma_0^{(p)} = 3 \times 10^{p-1} \times [0.4, 0, 0.5, 0, -0.3, 0, 0, 0, 0, 0, 0]^T$ if p is an odd number, otherwise $\Gamma_0^{(p)} = 7 \times 10^{p-1} \times [0.4, 0, 0.5, 0, -0.3, 0, 0, 0, 0, 0, 0]^T$. Thereinto, Fig. 7(a) manifests that the convergence time of $\|s(t)\|_2$ synthesized by the ARPTNSMC has barely changed when its initial value gets near $\Gamma_0^{(2)}$. That is, the upper bound of convergence time

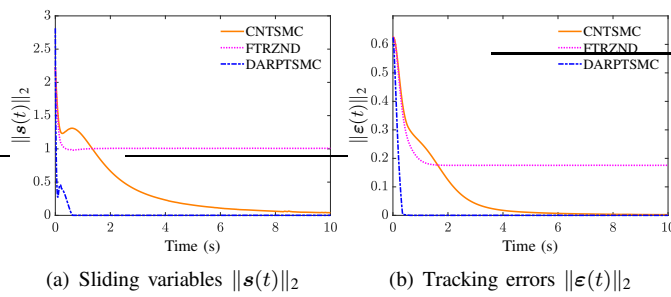


Fig. 10. Sliding variables $\|s(t)\|_2$ and tracking errors $\|\varepsilon(t)\|_2$ synthesized by three schemes when $\delta_j(t) = 3$.

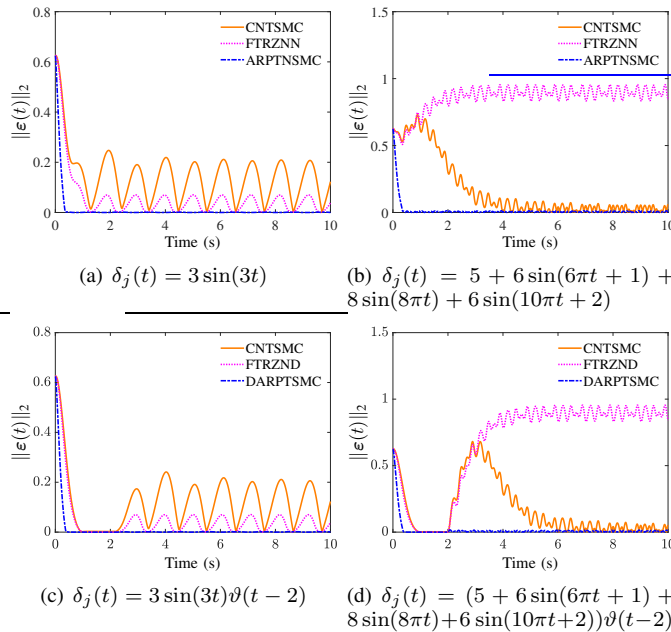


Fig. 11. Tracking errors $\|\varepsilon(t)\|_2$ synthesized by three schemes under different disturbances with $\vartheta(t)$ representing the Heaviside step function.

synthesized by the ARPTNSMC is unrelated to the initial state. It can be seen from Fig. 7(b) that, the smaller the predetermined parameter \mathcal{T}_p is, the smaller the convergence time of tracking error would be, which indicates that the parameter \mathcal{T}_p can indeed control the convergence time of tracking error.

2) *Robustness analysis*: The constant disturbance, sinusoidal disturbance, and hybrid sinusoidal disturbance are considered in order to test and verify robustness of the ARPTNSMC scheme. In Figs. 8 and 9, the butterfly-shaped trajectories, position, and attitude synthesized by these three schemes subjected to constant disturbance are illustrated. As shown in Figs. 8 and 9, only position and attitude trajectories synthesized by the FTRZNN cannot fit reference position and attitude trajectories, indicating that the CNTSMC and the ARPTNSMC schemes are robust to constant disturbance $\delta_j(t) = 3$. Besides, Fig. 10 draws sliding variables $\|s(t)\|_2$ and tracking errors $\|\varepsilon(t)\|_2$ synthesized by these three schemes. The findings provide substantial evidence that the ARPTNSMC scheme has stronger anti-disturbance ability to constant disturbance than the other two schemes.

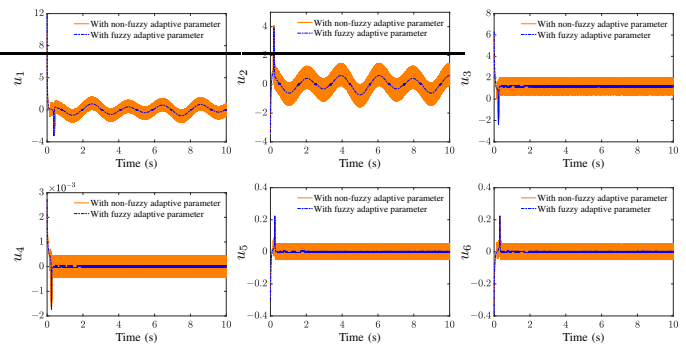


Fig. 12. Control inputs synthesized by the ARPTNSMC with fuzzy adaptive parameter or non-fuzzy adaptive parameter when $\delta_j(t) = 0$.

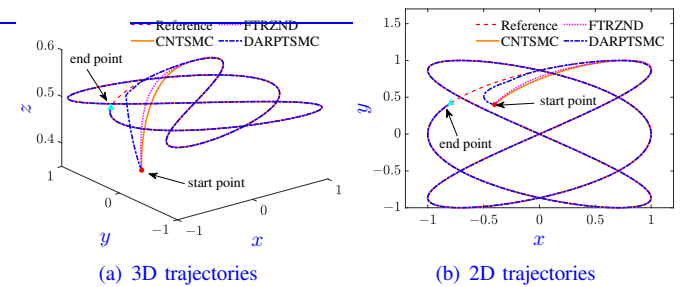


Fig. 13. Lissajous trajectories tracking of the quadrotor controlled by three schemes when $\delta_j(t) = 0$.

Finally, some additional time-varying disturbances are considered in Fig. 11. From Fig. 11(a), only $\|\varepsilon(t)\|_2$ synthesized by the ARPTNSMC reaches zero under disturbance $\delta_j(t) = 3 \sin(3t)$, whereas $\|\varepsilon(t)\|_2$ synthesized by the other two schemes exhibit apparent oscillations. In Fig. 11(b), even though $\|\varepsilon(t)\|_2$ synthesized by the three schemes exist certain oscillations under hybrid sinusoidal disturbance $\delta_j(t) = 5 + 6 \sin(6\pi t + 1) + 8 \sin(8\pi t) + 6 \sin(10\pi t + 2)$, the ARPTNSMC manifests the least oscillation. Besides, the above two kinds of disturbances are introduced into these models after 2 seconds. The results are exhibited in Figs. 11(c)-11(d), which is similar to those in Figs. 11(a)-11(b). Overall, these results reveal that the robustness of the ARPTNSMC scheme is better than the other schemes.

3) *Chattering analysis*: To verify the low-chattering of the ARPTNSMC, in the case of $\delta_j(t) = 0$, a comparative simulation is carried out when the fuzzy adaptive parameter ϱ in fuzzy adaptive PTAF (10) is replaced by constant c_3 , i.e.,

$$p_1(\xi) = \frac{4\lambda}{\mathcal{T}_p} (|\xi|^\alpha + |\xi|^\beta) \text{sign}(\xi) + c_3 \text{sign}(\xi) + \rho(\xi)\xi.$$

As shown in Fig. 12, the corresponding control inputs of the quadrotor controlled by the ARPTNSMC with fuzzy adaptive parameter or non-fuzzy adaptive parameter are exhibited when parameter $c_3 = 3$. More specifically, Fig. 12 indicates that the control inputs with fuzzy adaptive parameter is smoother and lower chattering than the control inputs with non-fuzzy parameter. Thus, the results demonstrate that the fuzzy adaptive parameter generated by the Takagi-Sugeno fuzzy logic system can suppress chattering.

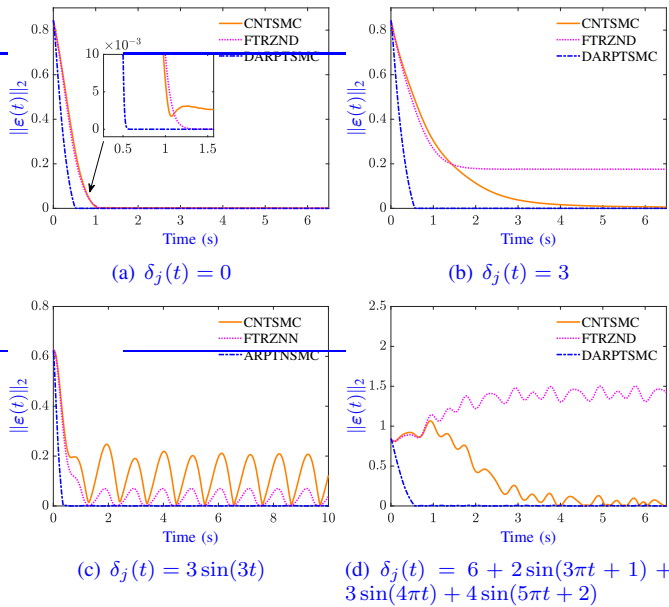


Fig. 14. Tracking errors $\|\varepsilon(t)\|_2$ synthesized by three schemes under different disturbances for Lissajous trajectory.

C. Lissajous Trajectory

In this part, a reference Lissajous trajectory is provided to further verify the effectiveness of the ARPTNSMC scheme. The reference Lissajous trajectory is as follows:

$$\begin{cases} x_d = \sin(3t + 1.5\pi), \\ y_d = \sin(2t), \\ z_d = 0.5, \end{cases}$$

and $\phi_d = \theta_d = \psi_d = 0.1$. The initial state is $\Gamma_0 = [-0.4, 0, 0.4, 0, 0.35, 0, -0.1, 0, 0.3, 0, 0.4, 0]^T$.

Firstly, Fig. 13 depicts Lissajous trajectories executed by three different control schemes. As shown in Figs. 13(a) and 13(b), the results in 3D and 2D trajectories reveal that the ARPTNSMC scheme possesses a quicker convergence speed than the other schemes when disturbance $\delta_j(t) = 0$. In Fig. 14, the errors synthesized by the three schemes under different disturbances for the Lissajous trajectory are displayed. Specifically, Fig. 14(a) exhibits that the error synthesized by the ARPTNSMC converges fastest under $\delta_j(t) = 0$, further illustrating the superiority of the ARPTNSMC scheme in convergence speed. In Fig. 14(b), even though the tracking errors synthesized by the ARPTNSMC and the CNTSMC can both converge under $\delta_j(t) = 3$, the error synthesized by the ARPTNSMC converges faster. Furthermore, as shown in Figs. 14(c) and 14(d), only the tracking error synthesized by the ARPTNSMC can converge under $\delta_j(t) = 3 \sin(3t)$ and $\delta_j(t) = 6 + 2 \sin(3\pi t + 1) + 3 \sin(4\pi t) + 4 \sin(5\pi t + 2)$, confirming its strong robustness. In general, the results in Figs. 13 and 14 verify that the ARPTNSMC scheme can track the Lissajous trajectory well.

VI. CONCLUSION

In this paper, a novel SMC scheme combining a dynamic adaptive parameter and a fuzzy adaptive parameter

under the framework of zeroing neural network has been presented and applied to position and attitude tracking of a quadrotor. Importantly, the theoretical analysis ensures not only the predefined-time reachability of the sliding surface but also the predefined-time convergence and robustness of the closed-loop system. Moreover, the butterfly trajectory and Lissajous trajectory tracking examples have confirmed that the closed-loop system controlled by the ARPTNSMC has better convergence and stronger robustness than those by the other schemes. In addition, a comparative simulation has been implemented to confirm that the control inputs with fuzzy adaptive parameter have led to lower chattering than those with non-fuzzy parameter. In the future, the developed fuzzy neural network scheme could be applied to the cooperative control of UAVs under the condition of delay.

REFERENCES

- [1] H. Shraim, A. Awada, and R. Youness, "A survey on quadrotors: Configurations, modeling and identification, control, collision avoidance, fault diagnosis and tolerant control," *IEEE Aerosp. Electron. Syst. Mag.*, vol. 33, no. 7, pp. 14–33, Jul. 2018.
- [2] W. Budiharto, E. Irwansyah, J. S. Suroso, A. Chowanda, H. Ngarianto, and A. A. S. Gunawan, "Mapping and 3D modelling using quadrotor drone and GIS software," *J. Big Data*, vol. 8, no. 48, pp. 1–12, Mar. 2021.
- [3] A. Deleforge, D. Di Carlo, M. Strauss, R. Serizel, and L. Marcenaro, "Audio-based search and rescue with a drone: Highlights from the IEEE signal processing cup 2019 student competition [SP competitions]," *IEEE Signal Proc. Mag.*, vol. 36, no. 5, pp. 138–144, Sep. 2019.
- [4] N. Koksals, H. An, and B. Fidan, "Backstepping-based adaptive control of a quadrotor UAV with guaranteed tracking performance," *ISA Trans.*, vol. 105, pp. 98–110, Oct. 2020.
- [5] D. Wang, Q. Pan, Y. Shi, J. Hu, and C. Zhao, "Efficient nonlinear model predictive control for quadrotor trajectory tracking: Algorithms and experiment," *IEEE Trans. Cybern.*, vol. 51, no. 10, pp. 5057–5068, Oct. 2021.
- [6] S. Wang, Y. Cao, T. Huang, Y. Chen, P. Li, and S. Wen, "Sliding mode control of neural networks via continuous or periodic sampling event-triggering algorithm," *Neural Netw.*, vol. 121, pp. 140–147, Jan. 2020.
- [7] A. Karimi, H. Akbari, S. Mousavi, and Z. Beheshtipour, "Design of an adaptive terminal sliding mode to control the PMSM chaos phenomenon," *Syst. Sci. Control. Eng.*, vol. 11, no. 1, p. 2207593, Jun. 2023.
- [8] W. Ji, Y. Jiang, X. Xie, and S. Wang, "Parameter-dependent functional observer-based finite-time adaptive memory ISMC for continuous LPV systems with unknown nonlinear functions," *Int. J. Syst. Sci.*, vol. 54, no. 13, pp. 2626–2646, Aug. 2023.
- [9] O. Mofid and S. Mobayen, "Adaptive sliding mode control for finite-time stability of quad-rotor UAVs with parametric uncertainties," *ISA Trans.*, vol. 72, pp. 1–14, Jan. 2018.
- [10] O. Mofid, S. Mobayen, C. Zhang, and B. Esakki, "Desired tracking of delayed quadrotor UAV under model uncertainty and wind disturbance using adaptive super-twisting terminal sliding mode control," *ISA Trans.*, vol. 123, pp. 455–471, Apr. 2022.
- [11] B. Li, W. Gong, Y. Yang, B. Xiao, and D. Ran, "Appointed fixed time observer-based sliding mode control for a quadrotor UAV under external disturbances," *IEEE Trans. Aerosp. Electron. Syst.*, vol. 58, no. 1, pp. 290–303, Feb. 2021.
- [12] Y. Jing, X. Wang, J. Heredia-Juesas, C. Fortner, C. Giacomo, R. Sipahi, and J. Martinez-Lorenzo, "PX4 simulation results of a quadcopter with a disturbance-observer-based and PSO-optimized sliding mode surface controller," *Drones*, vol. 6, no. 9, p. 261, Sep. 2022.
- [13] J. Fang, W. Liu, L. Chen, S. Lauria, A. Miron, and X. Liu, "A survey of algorithms, applications and trends for particle swarm optimization," *Int. J. Netw. Dyn. Intell.*, vol. 2, no. 1, pp. 24–50, Mar. 2023.
- [14] K. Guo, Y. Hu, Z. Qian, H. Liu, K. Zhang, Y. Sun, J. Gao, and B. Yin, "Optimized graph convolution recurrent neural network for traffic prediction," *IEEE Trans. Intell. Transp. Syst.*, vol. 22, no. 2, pp. 1138–1149, Feb. 2020.

- 1
2
3
4
5
6
7
8
9
10
11
12
13
14
15
16
17
18
19
20
21
22
23
24
25
26
27
28
29
30
31
32
33
34
35
36
37
38
39
40
41
42
43
44
45
46
47
48
49
50
51
52
53
54
55
56
57
58
59
- [15] X. Wang, Y. Sun, and D. Ding, "Adaptive dynamic programming for networked control systems under communication constraints: A survey of trends and techniques," *Int. J. Netw. Dyn. Intell.*, vol. 1, no. 1, pp. 85–98, Dec. 2022.
- [16] X. Li, M. Li, P. Yan, G. Li, Y. Jiang, H. Luo, and S. Yin, "Deep learning attention mechanism in medical image analysis: Basics and beyonds," *Int. J. Netw. Dyn. Intell.*, vol. 2, no. 1, pp. 93–116, Mar. 2023.
- [17] L. Jin, J. Yan, X. Du, X. Xiao, and D. Fu, "RNN for solving time-variant generalized Sylvester equation with applications to robots and acoustic source localization," *IEEE Trans. Ind. Inform.*, vol. 16, no. 10, pp. 6359–6369, Oct. 2020.
- [18] M. Yang, Y. Zhang, N. Tan, and H. Hu, "Concise discrete ZNN controllers for end-effector tracking and obstacle avoidance of redundant manipulators," *IEEE Trans. Ind. Inform.*, vol. 18, no. 5, pp. 3193–3202, May 2021.
- [19] M. Yang, Y. Zhang, Z. Zhang, and H. Hu, "Adaptive discrete ZND models for tracking control of redundant manipulator," *IEEE Trans. Ind. Inform.*, vol. 16, no. 12, pp. 7360–7368, Dec. 2020.
- [20] W. Li and Y. Pan, "A Dini-derivative-aided zeroing neural network for time-variant quadratic programming involving multi-type constraints with robotic applications," *IEEE Trans. Neural Netw. Learn. Syst.*, 2023, in press with doi: 10.1109/TNNLS.2023.3263263.
- [21] H. Lu, L. Jin, J. Zhang, Z. Sun, S. Li, and Z. Zhang, "New joint-drift-free scheme aided with projected ZNN for motion generation of redundant robot manipulators perturbed by disturbances," *IEEE Trans. Syst. Man Cybern. Syst.*, vol. 51, no. 9, pp. 5639–5651, Sep. 2019.
- [22] L. Xiao, L. Li, P. Cao, and Y. He, "A fixed-time robust controller based on zeroing neural network for generalized projective synchronization of chaotic systems," *Chaos Solitons Fractals*, vol. 169, p. 113279, Apr. 2023.
- [23] J. Jin, J. Zhu, L. Zhao, L. Chen, L. Chen, and J. Gong, "A robust predefined-time convergence zeroing neural network for dynamic matrix inversion," *IEEE Trans. Cybern.*, vol. 53, no. 6, pp. 3887–3900, Jun. 2023.
- [24] J. Jin, J. Zhu, L. Zhao, and L. Chen, "A fixed-time convergent and noise-tolerant zeroing neural network for online solution of time-varying matrix inversion," *Appl. Soft Comput.*, vol. 130, p. 109691, Nov. 2022.
- [25] Z. Zhang, B. Zhou, L. Zheng, Z. Zhang, C. Song, and H. Pei, "A varying-parameter adaptive multi-layer neural dynamic method for designing controllers and application to unmanned aerial vehicles," *IEEE Trans. Intell. Transp. Syst.*, vol. 22, no. 8, pp. 4876–4888, Aug. 2020.
- [26] Z. Zhang and Z. Yan, "An adaptive fuzzy recurrent neural network for solving the nonrepetitive motion problem of redundant robot manipulators," *IEEE Trans. Fuzzy Syst.*, vol. 28, no. 4, pp. 684–691, Apr. 2020.
- [27] J. Zhang, L. Jin, and Y. Wang, "Collaborative control for multimanipulator systems with fuzzy neural networks," *IEEE Trans. Fuzzy Syst.*, vol. 31, no. 4, pp. 1305–1314, Apr. 2022.
- [28] J. Dai, X. Yang, L. Xiao, L. Jia, X. Liu, and Y. Wang, "Design and analysis of a self-adaptive zeroing neural network for solving time-varying quadratic programming," *IEEE Trans. Neural Netw. Learn. Syst.*, vol. 34, no. 10, pp. 7135–7144, Oct. 2023.
- [29] L. Jia, L. Xiao, J. Dai, and Y. Wang, "Intensive noise-tolerant zeroing neural network based on a novel fuzzy control approach," *IEEE Trans. Fuzzy Syst.*, vol. 31, no. 12, pp. 4350–4360, Dec. 2023.
- [30] V. N. Katsikis, P. S. Stanimirović, S. D. Mourtas, L. Xiao, D. Karabašević, and D. Stanujkić, "Zeroing neural network with fuzzy parameter for computing pseudoinverse of arbitrary matrix," *IEEE Trans. Fuzzy Syst.*, vol. 30, no. 9, pp. 3426–3435, Sep. 2021.
- [31] K. Lu and Y. Xia, "Adaptive attitude tracking control for rigid spacecraft with finite-time convergence," *Automatica*, vol. 49, no. 12, pp. 3591–3599, Dec. 2013.
- [32] J. Zhang, W. Zhao, G. Shen, and Y. Xia, "Disturbance observer-based adaptive finite-time attitude tracking control for rigid spacecraft," *IEEE Trans. Syst. Man Cybern. Syst.*, vol. 51, no. 11, pp. 6606–6613, Nov. 2021.
- [33] N. P. Nguyen, H. Oh, and J. Moon, "Continuous nonsingular terminal sliding-mode control with integral-type sliding surface for disturbed systems: Application to attitude control for quadrotor UAVs under external disturbances," *IEEE Trans. Aerosp. Electron. Sys.*, vol. 58, no. 6, pp. 5635–5660, Dec. 2022.
- [34] J. Dai, Y. Li, L. Xiao, and L. Jia, "Zeroing neural network for time-varying linear equations with application to dynamic positioning," *IEEE Trans. Ind. Inform.*, vol. 18, no. 3, pp. 1552–1561, Mar. 2021.
- [35] L. Xiao, Y. Cao, J. Dai, L. Jia, and H. Tan, "Finite-time and predefined-time convergence design for zeroing neural network: Theorem, method, and verification," *IEEE Trans. Ind. Inform.*, vol. 17, no. 7, pp. 4724–4732, Jul. 2020.
- [36] C. Hu, H. He, and H. Jiang, "Fixed/preassigned-time synchronization of complex networks via improving fixed-time stability," *IEEE Trans. Cybern.*, vol. 51, no. 6, pp. 2882–2892, Jun. 2020.
- [37] C. Hu and H. Jiang, "Special functions-based fixed-time estimation and stabilization for dynamic systems," *IEEE Trans. Syst. Man Cybern. Syst.*, vol. 52, no. 5, pp. 3251–3262, May 2021.
- [38] Z. Qi, Y. Ning, L. Xiao, Y. He, J. Luo, and B. Luo, "Predefined-time zeroing neural networks with independent prior parameter for solving time-varying plural Lyapunov tensor equation," *IEEE Trans. Neural Netw. Learn. Syst.*, 2023, in press with doi: 10.1109/TNNLS.2022.3233050.
- [39] G. E. Andrews, R. Askey, R. Roy, R. Roy, and R. Askey, *Special functions*. Cambridge university press Cambridge, 1999, vol. 71.
- [40] F. Chen, R. Jiang, K. Zhang, B. Jiang, and G. Tao, "Robust backstepping sliding-mode control and observer-based fault estimation for a quadrotor UAV," *IEEE Trans. Ind. Electron.*, vol. 63, no. 8, pp. 5044–5056, Aug. 2016.
- [41] L. Xu, D. Guo, and H. Ma, "Cascade active disturbance rejection control for quadrotor UAV," in *Proc. 38th Chin. Control Conf. (CCC 2019)*. IEEE, Oct. 2019, pp. 8044–8048.
- [42] L. Xiao, K. Li, and M. Duan, "Computing time-varying quadratic optimization with finite-time convergence and noise tolerance: A unified framework for zeroing neural network," *IEEE Trans. Neural Netw. Learn. Syst.*, vol. 30, no. 11, pp. 3360–3369, Nov. 2019.
- [43] L. Yu, G. He, X. Wang, and S. Zhao, "Robust fixed-time sliding mode attitude control of tilt trirotor UAV in helicopter mode," *IEEE Trans. Ind. Electron.*, vol. 69, no. 10, pp. 10322–10332, Oct. 2021.
- [44] S. Ma and Y. Li, "Adaptive fuzzy fault-tolerant control for active seat suspension systems with full-state constraints," *Syst. Sci. Control. Eng.*, vol. 11, no. 1, p. 2153391, Jan. 2023.
- [45] Y. Wang, Z. Wang, L. Zou, L. Ma, and H. Dong, "Ultimately bounded PID control for T-S fuzzy systems under flexray communication protocol," *IEEE Trans. Fuzzy Syst.*, vol. 31, no. 12, pp. 4308–4320, Dec. 2023.
- [46] E. S. Tognetti and T. M. Linhares, "Local dynamic output feedback control of saturated discrete-time TS fuzzy systems with partially measured premise variables," *Int. J. Syst. Sci.*, vol. 54, no. 14, pp. 2784–2798, Aug. 2023.
- [47] Q. Hu and B. Zheng, "An efficient Takagi-Sugeno fuzzy zeroing neural network for solving time-varying Sylvester equation," *IEEE Trans. Fuzzy Syst.*, vol. 31, no. 7, pp. 2401–2411, Jul. 2022.